5848 *Chem. Mater.* **2009,** *21,* 5848–5859
DOI:10.1021/cm902450q

CHEMISTRY OF MATERIALS
Article

Intercalation/Deintercalation of Oxygen: A Sequential Evolution of Phases in Ce_2O_3/CeO_2-ZrO_2 Pyrochlores

S. Nagabhusan Achary,*,† Sanjay K. Sali,‡ Narendra K. Kulkarni,‡ P. Siva Ram Krishna,§ Anil B. Shinde,§ and Avesh K. Tyagi*,†

†*Chemistry Division, and* ‡*Fuel Chemistry Division, and* §*Solid State Physics Division, Bhabha Atomic Research Centre, Mumbai 400 085, India*

Received August 11, 2009. Revised Manuscript Received November 1, 2009

In this paper, we report the structural and compostional variation of $Ce_2Zr_2O_7$ pyrochlore under a controlled oxidation/reduction process. On oxidation $Ce_2Zr_2O_7$ transforms to $Ce_2Zr_2O_8$ via an intermediate lattice at $Ce_2Zr_2O_{7.5}$. Crystal structures of the $Ce_2Zr_2O_7$, $Ce_2Zr_2O_{7.5}$, and $Ce_2Zr_2O_8$ have been determined accurately from the neutron diffraction data of polycrystalline samples. The retention of cubic pyrochlore-type arrangements is observed even up to the fully oxidized $Ce_2Zr_2O_8$ composition. The unit cell parameters systematically decreased from $Ce_2Zr_2O_7$ (10.6924(3) Å) to $Ce_2Zr_2O_8$ (10.5443(2) Å). All three compositions retain the original pyrochlore-type cation ordering without any intermixing Ce and Zr atoms. All three structures can be explained as cubically coordinated metal atoms, which share the edge of their AO_8 polyhedra similar to that in the fluorite lattice. The transformation from $Ce_2Zr_2O_7$ to $Ce_2Zr_2O_8$ systematically lowers the symmetry from $Fd\bar{3}m$ to $P2_13$. A complete oxidation of Ce^{3+} to Ce^{4+} is observed, in contrast to the kinetically and sterically hindered oxidation proposed earlier. The deep crystallographic insights associated with the oxygen intercalation and deintercalation process in Ce_2O_3/CeO_2-ZrO_2 will have immense importance in the development and understanding of new oxygen storage capacitors.

1. Introduction

The pyrochlore lattice has been a subject of great interest due to its several important physical properties like high oxygen mobility,[1] catalytic properties,[2] stable and robust host lattice for nuclear waste immobilization,[3] and inert matrix fuel for nuclear technology.[4] In addition, the rich crystal chemistry originating from the cation and anion stoichiometry and compositions has also generated interest for extensive crystallographic studies in pyrochlore-type materials.[5] The general composition of the pyrochlore lattice can be written as $A_2B_2X_6Y$, where the A site cation is cubically coordinated with the X and Y anions while the B site ion is octahedrally coordinated with X anions. This preferential coordination of the cations restricts their choice by radius ratio (r_A/r_B = 1.46−1.80).[5] Thus, the pyrochlore lattice is formed only with cations of appropriate ionic radii and charge combinations. However, the radius ratio limit can be extended further under high-pressure synthetic conditions.[6] Lower values of the radius ratio preferentially favor the anion-deficient fluorite lattice due to anti site formation of cations. The pyrochlore lattice can be explained as a cation-ordered anion-deficient fluorite lattice. The ordering process transforms the symmetry of the lattice from $Fm\bar{3}m$ to $Fd\bar{3}m$ with doubling of the unit cell parameter. The two types of cations, namely, cubically coordinated A atoms and octahedrally coordinated B atoms occupy 16d and 16c sites of space group $Fd\bar{3}m$, while the anions X and Y occupy the 48f and 8b sites, respectively. The anions and vacancy ordering in these materials play a significant role in governing their stabilities and physical properties under nonambient conditions of temperature and pressure.[7]

Structural and thermophysical properties of pyrochlore-type rare-earth zirconates and hafnates (3:4 charge combination of A and B) have been studied in the interest of fixation of actinides from high-level nuclear waste (HLW).[3,8] Further attention on these materials has been widened due to several other important physical properties like oxide ion mobility,[1,9,10] thermodynamic properties,[11] etc. Several zirconia-based pyrochlores find

*To whom correspondence should be addressed. Phone: 0091-22-25592328. Fax: 0091-22-25505151. E-mail: sachary@barc.gov.in/aktyagi@barc.gov.in.

(1) Wuensch, B. J.; Eberman, K. W.; Heremans, C.; Ku, E. M.; Onnerud, P.; Yeo, E. M.E.; Haile, S. M.; Stalick, J. K.; Jorgensen, J. D. *Solid State Ionics* **2000**, *129*, 111.
(2) Loong, C. −K.; Richardson, J. W.Jr; Ozawa, M. *J. Catal.* **1995**, *157*, 636.
(3) Ewing, R. C. *Proc. Natl. Acad. Sci. U.S.A.* **1999**, *96*, 3432.
(4) Ferguson, K. *Trans. Am. Nucl. Soc.* **1996**, *75*, 75.
(5) Subramanian, M. A.; Aravamudan, G.; Subba Rao, G. V. *Prog. Solid State Chem.* **1983**, *15*, 55.
(6) Sleight, A. W. Inorg. Chem. **1968**, *7*, 1704; 1969, *8*, 2039.
(7) Zhang, F. X.; Wang, J. W.; Lian, J.; Lang, M. K.; Becker, U.; Ewing, R. C. *Phys. Rev. Lett.* **2008**, *100*, No. 045503.
(8) Ewing, R. C.; Weber, W. J.; Lian, J. *J. Appl. Phys.* **2004**, *95*, 5949.
(9) Mandal, B. P.; Banerji, A.; Sathe, V.; Deb, S. K.; Tyagi, A. K. *J. Solid State Chem.* **2007**, *180*, 2643.
(10) Mandal, B. P.; Deshpande, S. K.; Tyagi, A. K. *J. Mater. Res.* **2008**, *23*, 911.
(11) Popa, K.; Konings, R. J. M.; Wastin, F.; Colineau, E.; Magnani, N.; Raison, P. E. *J. Phys. Chem. Solids* **2008**, *68*, 70.

 Published on Web 11/20/2009

applications as thermal barrier coatings in space craft and high-temperature turbines.[11] Among the rare-earth zirconates, $Ce_2Zr_2O_7$ bears additional interest due to the catalytic application of CeO_2-ZrO_2 in several chemical processes in industry and automobiles.[12−22] CeO_2 and CeO_2 coupled with various metal or metal oxides have been used as efficient catalysts for various applications like water gas shift, oxidation of CO and hydrocarbons, and dissociation of methane.[23−27] Local structures as well as surface and bulk oxygen vacancies in CeO_2 play crucial roles for its oxygen storage and release behaviors.[28,29] Various compositions in the CeO_2-ZrO_2 system have been extensively investigated for such applications due to their enhanced redox properties.[12−22,30−43] Reports on the redox behavior of CeO_2 and CeO_2-ZrO_2 solid solutions suggest that the reduction of Ce^{4+} to Ce^{3+} is favored in the case of ZrO_2-containing compositions.[20−22,33−42] The mechanistic studies of such catalytic processes revealed that the oxygen stoichiometry between CeO_2 and Ce_2O_3 plays a vital role in $Ce_2Zr_2O_7$ for storing and releasing of oxygen at relatively lower temperature (673−1073 K) by valence fluctuation of cerium.[20−22,27−30,43−45] Thus, the crystallographic and thermodynamic studies of the $CeO_2-Ce_2O_3-ZrO_2$ system are essential to understand the process of oxygen gain and release.

Phase evolution studies in the CeO_2-ZrO_2 system under reducing and oxidizing conditions have drawn attention in several reports.[38−53] Reports indicate that the redox behavior of the CeO_2-ZrO_2 phases is strongly related to the pretreatment, like mild or severe reduction or oxidation conditions.[21,22,34−43] The reduction behavior of fluorite-type $Ce_{0.5}Zr_{0.5}O_2$ revealed a distinct temperature for reduction for sample pretreated for a severe oxidation (oxidation ∼1273 K) or a mild oxidation (oxidation at 700 K) after a severe reduction around 1273 K.[21,22,30,33−35,38,39] In situ microstructural investigations on CeO_2-ZrO_2 samples indicate the textural variation and secondary pyrochlore-like phase formation under the reducing conditions.[21,22,30,33−35,39−44] X-ray diffraction and electron microscopic studies on oxidized samples of $Ce_2Zr_2O_7$ revealed several new phases, like $Ce_2Zr_2O_{7+x}$, with x ranging from 0.3 to 1.0[41,45−53] Extensive in depth HREM and dark field scanning TEM studies on a closely related composition, $Ce_{0.68}Zr_{0.32}O_2$, treated with various redox cycle conditions revealed the formation of a cation-ordered pyrochlore-type lattice.[44] Similar observations have also been reported by *in situ* Raman and XRD studies on redox-treated samples of $Ce_{0.5}Zr_{0.5}O_2$.[22,33,39,43] The evolution of crystal structures during the oxidation process of $Ce_2Zr_2O_7$ have also been

(12) Yamamoto, T.; Suzuki, A.; Nagai, Y.; Tanabe, T.; Dong, F.; Inada, Y.; Nomura, M.; Tada, M.; Iwasawa, Y. *Angew. Chem., Int. Ed.* **2007**, *46*, 9253.
(13) Yeste, M. P.; Hernández, J. C.; Bernal, S.; Blanco, G.; Calvino, J. J.; Párez-Omil, J. A.; Pintado, J. M. *Catal. Today* **2009**, *141*, 409.
(14) Di Monte, R.; Fornasiero, P.; Kašpar, J.; Graziani, M.; Gatica, J. M.; Bernal, S.; Gomez-Herrero, A. *Chem. Commun.* **2000**, No. 21, 2167.
(15) Montini, T.; De Rogatis, L.; Gombac, V.; Fornasiero, P.; Graziani, M. *Appl. Catal., B* **2007**, *71*, 125.
(16) Hickey, N.; Fornasiero, P.; Di Monte, R.; Kašpar, J.; Gonzalez-Velasco, J. R.; Gutirrez-Ortiz, M. A.; Gonzlez-Marcos, M. P.; Gatica, J. M.; Bernal, S. *Chem. Commun.* **2004**, No. 10, 196.
(17) Gatica, J.; Fornasiero, P.; Kašpar, J.; Lesage, T.; Aiello, S.; Daturi, M. *Phys. Chem. Chem. Phys.* **2002**, *4*, 381.
(18) Fornasiero, P.; Kašpar, J.; Montini, T.; Graziani, M.; Dal Santo, V.; Psaro, R.; Recchia, S. *J. Mol. Catal. A* **2003**, *204−205*, 683.
(19) Bernal, S.; Blanco, G.; Calvino, J. J.; Gatica, J. M.; Párez Omil, J. A.; Pintado, J. M. *Top. Catal.* **2004**, *28*, 31.
(20) Vlaic, G.; Fornasiero, P.; Geremia, S.; Kašpar, J.; Graziani, M. *J. Catal.* **1997**, *168*, 386.
(21) Bernal, S.; Blanco, G.; Calvino, J. J.; Hernández,, J. C.; Pérez-Omil, J. A.; Pintado, J. M.; Yeste, M. P. *J. Alloys Compd.* **2008**, *451*, 521.
(22) Montini, T.; Baares, M. A.; Hickey, N.; Di Monte, R.; Fornasiero, P.; Kašpar, J.; Graziani, M. *Phys. Chem. Chem. Phys.* **2004**, *6*, 1.
(23) Fu, Q.; Saltsburg, H.; Flytzani-Stephanopoulos, M. *Science* **2003**, *301*, 935.
(24) Deluga, G. A.; Salge, J. R.; Schmidt, L. D.; Verykios, X. E. *Science* **2004**, *301*, 993.
(25) Knapp, D.; Ziegler, T. *J. Phys. Chem. C* **2008**, *112*, 17311.
(26) Rodriguez, J. A.; Ma, S.; Liu, P.; Hrbek, J.; Evans, J.; Parez, M. *Science* **2007**, *318*, 1757.
(27) Trovarelli, A. Ed. *Catalysis by Ceria and Related Materials*; Imperial College Press; London, 2000.
(28) Campbell, C. T.; Peden, C. H. F. *Science* **2005**, *309*, 713.
(29) Esch, F.; Fabris, S.; Zhou, L.; Montini, T.; Africh, C.; Fornasiero, P.; Comelli, G.; Rosei, R. *Science* **2005**, *309*, 752.
(30) Yeste, M. P.; Hernández, J. C.; Trasobares, S.; Bernal, S.; Blanco, G.; Calvino, J. J.; Pérez-Omil, J. A.; Pintado, J. M. *Chem. Mater.* **2008**, *20*, 5107.
(31) Baker, R. T.; Bernal, S.; Blanco, G.; Cordón, A. M.; Pintado, J. M.; Rodríguez-Izquierdo, J. M.; Fally, F.; Perrichon, V. *Chem. Commun.* **1999**, 149..
(32) Colón,, G.; Valdivieso, F.; Pijolat, M.; Baker, R. T.; Calvino, J. J.;; Bernal, S. *Catal. Today* **1999**, *50*, 271.
(33) Fornasiero, P.; Fonda, E.; Di Monte, R.; Vlaic, G.; Kašpar, J.; Graziani, M. *J. Catal.* **1999**, *187*, 177.
(34) Fornasiero, P.; Montini, T.; Graziani, M.; Kašpar, J.; Hungrı́, A. B.; Martı́ ez-Arias, A.; Conesa, J. C. *Phys. Chem. Chem. Phys.* **2002**, *4*, 149.
(35) Yeste, M. P.; Hernández, J. C.; Bernal, S.; Blanco, G.; Calvino, J. J.; Pérez-Omil, J. A.; Pintado, J. M. *Chem. Mater.* **2006**, *18*, 2750.
(36) Kašpar, J.; Di Monte, R.; Fornasiero, P.; Graziani, M.; Bradshaw, H.; Norman, C. *Top. Catal.* **2001**, *16−17*, 83.
(37) Di Monte, R.; Fornasiero, P.; Desinan, S.; Kašpar, J.; Gatica, J. M.; Calvino, J. J.; Fonda, E. *Chem. Mater.* **2004**, *16*, 4273.
(38) Fornasiero, P.; Balducci, G.; Di Monte, R.; Kăspar, J.; Sergo, V; Gubitosa, G.; Ferrero, A.; Graziani, M. *J. Catal.* **1996**, *164*, 173.
(39) Alessandri, I.; Bañres, M. A.; Depero, L. E.; Ferroni, M.; Fornasiero, P.; Gennari, F. C.; Hickey, N.; Martinez-Huerta, M. V.; Montini, T. *Top. Catal.* **2006**, *41*, 35.
(40) Sasaki, T.; Ukyo, Y.; Suda, A.; Sugiura, M.; Kuroda, K.; Arari, S.; Saka, H. *J. Ceram. Soc. Jpn.* **2003**, *111*, 382.
(41) Masui, T.; Ozaki, T.; Adachi, G.-y.; Kang, A.; Eyring, L. *Chem. Lett.* **2000**, *29*, 840.
(42) Suda, A.; Ykyo, Y.; Sobukawa, H.; Sasaki, T.; Nagai, Y.; Tanabe, T.; Sugiura, M. *J. Ceram. Soc. Jpn.* **2004**, *112*, 586.
(43) Montini, T.; Hickey, N.; Fornasiero, P.; Graziani, M.; Banares, M. A.; Martinez-Huerta, M. V.; Alessandri, I.; Depero, L. E. *Chem. Mater.* **2005**, *17*, 1157.
(44) Pérez-Omil, J. A.; Bernal, S.; Calvino, J. J.; Hernández, J. C.; Mira, C.; Rodríguez-Luque, M. P.; Erni, R.; Browning, N. D. *Chem. Mater.* **2005**, *17*, 4282.
(45) Masui, T.; Ozaki, T.; Adachi, G.-y.; Kang, Z.; Eyring, L.; Sasaki, T.; Ukyo, Y.; Kuroda, K.; Arai, S.; Saka, H. *J. Electron Microsc.* **2003**, *52*, 309.
(46) Arai, S.; Muto, S.; Sasaki, T.; Ukyo, Y.; Kuroda, K.; Saka, H. *Electrochem. Solid-State Lett.* **2006**, *9*, E1–E3.
(47) Arai, S.; Muto, S.; Sasaki, T.; Tatsumi, K.; Ukyo, Y.; Kuroda, K.; Saka, H. *Solid State Commun.* **2005**, *135*, 664.
(48) Arai, S.; Muto, S.; Murai, J.; Sasaki, T.; Ukyo, Y.; Kuroda, K.; Saka, H. *Mater. Trans.* **2004**, *45*, 2951.
(49) Thomson, J. B.; Armstrong, A. R.; Bruce, P. G. *J. Am. Chem. Soc.* **1996**, *118*, 11129.
(50) Thomson, J. B.; Armstrong, A. R.; Bruce, P. G. *J. Solid State Chem.* **1999**, *148*, 56.
(51) Sasaki, T.; Ukyo, Y.; Kuroda, K.; Arai, S.; Muto, S.; Saka, H. *J. Ceram. Soc. Jpn.* **2004**, *112*, 440.
(52) Baidya, T.; Hegde, M. S.; Gopalakrishnan, J. *J. Phys. Chem. B* **2007**, *111*, 5149.
(53) Kishimoto, H.; Takahisa, O.; Otsuka-Yao-Matsuo, S.; Ueda, K.; Hosono, H.; Kawazoe, H. *J. Alloys Compd.* **2000**, *312*, 94.

reported by microscopic and electron energy loss spectroscopy.[40,41,45−51] Baidya et al.[52] reported the formation of $Ce_2Zr_2O_7$ and $Ce_2Zr_2O_{6.2}$ by the reduction of fluorite type CeO_2-ZrO_2 solid solution at relatively lower temperature (~1100 K). A detailed characterization of oxygen stioichiometry was reported by Sasaki et al.[40] from thermogravimetric studies. The crystal structures of some of the oxygen-rich pyrochlore-type compositions, namely, $Ce_2Zr_2O_{7.34}$,[49] $Ce_2Zr_2O_{7.44}$ and $Ce_2Zr_2O_{7.5}$,[40,46,51] $Ce_2Zr_2O_{7.97}$,[50] and $Ce_2Zr_2O_8$,[53] have been reported in literature. Sasaki et al.[51] have discussed the crystal structure of $Ce_2Zr_2O_7$ and its oxidized product $Ce_2Zr_2O_{7.5}$ from powder XRD data. The anion distribution in $Ce_2Zr_2O_7$ reported by the Sasaki et al.[51] is drastically different from that reported by Baidya et al.[52] In all these structures, cations form an ordered sublattice, while the anions form a defective sublattice. However, the fully disordered cation phase of $Ce_2Zr_2O_8$ has been reported to be cubic (fluorite),[52] as well as metastable tetragonal (t and t′) structures.[54−56]

The structural transformation and crystallographic studies on the cation-ordered oxygen-rich pyrochlore lattices reported by Sasaki et al.[51] and Kishimoto et al.[53] are mainly based on the powder X-ray diffraction data. Sasaki et al.[51] have explained the crystal structure of $Ce_2Zr_2O_{7.5}$ with partially occupied anion sites retaining the original pyrochlore-like cation-ordered face centered ($F\bar{4}3m$) lattice. From powder neutron diffraction studies, Thomson et al. have reported an anion filled $Fd\bar{3}m$ pyrochlore lattice for the composition $Ce_2Zr_2O_{7.34}$.[49] Kishimoto et al.[53] reported that the pyrochlore ($Fd\bar{3}m$) lattice of $Ce_2Zr_2O_7$ composition transforms to primitive cubic ($P2_13$) lattice at composition $Ce_2Zr_2O_8$ (denoted as κ-$CeZrO_4$). However, powder neutron diffraction data of a closely related composition ($Ce_2Zr_2O_{7.97}$) was reported on the basis of a rhombohedral ($R\bar{3}m$) lattice.[50] The superstructure reflections of the pyrochlore lattice mainly originated from the cation ordering, while weak additional reflections can arise due to the anion nonstoichiometry. Such anion stoichiometry related weak reflections can rarely be observed in X-ray diffraction patterns. Further, the atomic arrangements, in particular the location and occupancies of lighter atoms in presence of heavy scatterers like Ce and Zr, cannot be determined accurately from X-ray diffraction data due to monotonic decrease of scattering amplitudes of X-rays with decreasing atomic number. In order to follow the structural transformation due to the light atoms (oxygen) as well as location and occupancies of anions in such anion-rich pyrochlores, neutron diffraction studies are superior to the XRD studies, due to comparable scattering lengths of oxygen, Ce, and Zr ($b_O = 0.580 \times 10^{-12}$ cm, $b_{Ce} = 0.484 \times 10^{-12}$ cm, and $b_{Zr} = 0.716 \times 10^{-12}$ cm). Thus, the oxygen position, stoichiometry, and shift-induced variations of crystal and defect structures can be resolved accurately from the neutron diffraction studies. In particular, the CeO_2 system offers a special advantage over other rare-earth-based compounds due to the multivalent nature and lower neutron absorption cross section of Ce. In the present powder neutron diffraction studies, we delineated the exact stoichiometry and location of the anions with an objective to correlate the pyrochlore to oxygen-rich pyrochlore lattice. The detailed results of these studies are presented in this paper.

2. Experimental Section

The precursor $Ce_2Zr_2O_7$ for the $Ce_2Zr_2O_8$ composition was prepared by the gel combustion method from the corresponding metal nitrates ($Ce(NO_3)_3 \cdot 6H_2O$, 99.999%, Alfa Aesar; $ZrO(NO_3)_2 \cdot xH_2O$, 99.99%, Aldrich) using glycerol as a fuel. Appropriate amounts of standard solutions of zirconium nitrate and cerium nitrate were mixed. The water content in $ZrO(NO_3)_2 \cdot xH_2O$ is confirmed from the weight loss in thermogravimetry. To this solution, glycerol (about 5% v/v) was added followed by evaporation to near dryness on a hot plate to form a transparent colorless gel. On further heating on the hot plate, the gel undergoes an auto-ignition process forming a floppy mass. The obtained powder was heated in air at 1073 K to remove residual carbon and any other volatile materials. The calcined powder was pressed into pellets of 10 mm diameter using a tungsten carbide cast and hydraulic press. The cold-pressed pellets were heated under a flowing atmosphere of 8% v/v hydrogen−argon gas mixture (flow rate 200 mL/min) at 1673 K for 50 h, with intermittent grinding and pelletizing every 24 h.

The product obtained after final heating was characterized by powder XRD data recorded on a STOE X-ray diffractometer, using monochromatized Cu $K\alpha_1$ radiation (λ = 1.5406 Å). This sample was used as a precursor for the preparation of other compositions. The oxidation behavior of $Ce_2Zr_2O_7$ was studied by thermogravimetry (TG) using a Mettler thermoanalyzer (model TGA/SDTA851^e/MT5/LF1600) in dry air. The thermoanalyzer was calibrated from the mass loss of $CaC_2O_4 \cdot H_2O$ to CaO during heating to 1273 K. The thermograms were recorded by heating about 100 mg of sample on the thermobalance at a heating rate of 10 K/min up to 1073 K. For the preparation of a batch of about 10 g of $Ce_2Zr_2O_{7.5}$ and $Ce_2Zr_2O_8$, optimized heating conditions obtained from the thermogravimetry were used. The formation of these phases was confirmed by comparing the weight of the product and oxidation data of thermogravimetric studies, as well as XRD data analyses.

About 10 g of each sample was packed in a vanadium can of 1 cm diameter and 5 cm height. The neutron diffraction data were collected with a linear 5-PSD-based Debye−Scherrer-type powder diffractometer installed at 100 MW_{th} Dhruva Research Reactor, BARC, Mumbai, in the 2θ range of 5−140°. The total data collection time for each sample was about 24 h. Details of the neutron diffraction data collection parameters are given in Table 1.

The detailed structural analyses of the three compositions, namely, $Ce_2Zr_2O_7$, $Ce_2Zr_2O_{7.5}$, and $Ce_2Zr_2O_8$ were carried by Rietveld refinement of the powder neutron diffraction (ND) data using the GSAS software package.[57] The diffraction peaks

(54) Yashima, M.; Sasaki, S.; Kakihana, M.; Yamaguchi, Y.; Arashi, H.; Yoshimura, M. *Acta Crystallogr.* **1994**, *B50*, 663.
(55) Omata, T.; Kishimoto, H.; Otsuka-Yao-Matsuo, S.; Ohtori, N.; Umesaki, N. *J. Solid State Chem.* **1999**, *147*, 573.
(56) Otsuka-Yao-Matsuo, S.; Omata, T.; Izu, N.; Kishimoto, H. *J. Solid State Chem.* **1998**, *138*, 47.
(57) Larson, A. C.; van Dreele, R. B. GSAS: General Structure Analysis System, Los Alamos National Laboratory, Report LA-UR 86-748, **2000**.

Table 1. The Instrumental and Data Collection Parameters for Neutron Diffraction

diffractometer	Debye−Scherrer
radiation	1.249 Å
source	100 MWt Dhruva Research Reactor, BARC, Mumbai
monochromator (diffracted beam)	Ge single crystal (331 face)
detector	5- linear PSD array
2θ range (deg)	5−140
scan time	24 h
temperature and pressure	300 K, 1 atm

Table 2. Refined Unit Cell Parameters for $Ce_2Zr_2O_{7+x}$ (x = 0.0, 0.5, and 1.0)

parameters	compositions		
molecular formula	$Ce_2Zr_2O_7$	$Ce_2Zr_2O_{7.52}$[a]	$Ce_2Zr_2O_8$
color	black	gray	bright yellow
crystal system	cubic	cubic	cubic
space group	$Fd\bar{3}m$ (No. 227)	$F\bar{4}3m$ (No. 216)	$P2_13$ (No. 198)
a (Å)	10.6924(3)	10.6199(2)	10.5443(2)
V (Å^3)	1222.43(11)	1197.74(6)	1172.34(6)
density (calcd), g/cm^3	6.245	6.466	6.693
R_p, R_{wp}	0.0714, 0.0533	0.0597, 0.0447	0.0664, 0.0500
χ^2	3.972	2.928	3.947
R_F^2	0.0717	0.0421	0.0519

[a] Composition derived from the refinement.

were modeled using the pseudo-Voigt profile function. The background was fitted with the shifted Chebyschev polynomial function. Initially, diffractometer zero, sample displacement, and background parameters, along with the scale, were refined with the unit cell parameters obtained from the X-ray diffraction studies. Subsequently, the unit cell parameters, half-width (U, V, and W), and mixing (η) parameters of the pseudo-Voigt function were refined. The peak asymmetry correction was also included in the refinements. After a proper match in the profile was obtained, the positional parameters and overall thermal parameters were refined. Subsequently, the individual isotropic thermal parameters were refined. The goodness of the refinements was observed by the residuals (R-values) and difference plots. The details of the refined parameters for the studied compositions are given in Tables 2 and 3.

3. Results and Discussion

The powder XRD pattern of $Ce_2Zr_2O_7$ prepared by reduction of the combustion synthesized product in Ar/8%H_2 atmosphere at 1673 K showed superstructure reflections attributable to the $Fd\bar{3}m$ symmetry of a typical pyrochlore lattice. Under reducing conditions, CeO_2 undergoes simultaneous reduction (Ce^{4+} to Ce^{3+}) and reaction with ZrO_2 to form a pyrochlore-type phase at this temperature. According to the theromodynamic data of the Ce−O system, the reduction of CeO_2 to Ce_2O_3 can occur at temperatures above 1273 K and low oxygen partial pressure ($\sim 10^{-20}$ bar).[58] In the present study, that is, in 8% H_2 under an argon atmosphere, CeO_2 reduces to Ce_2O_3 prior to reaction with ZrO_2 at 1673 K. The oxygen content of the $Ce_2Zr_2O_7$ was estimated by the oxidation behavior of Ce^{3+} to Ce^{4+} on a thermobalance. A typical thermogram (TG/DTG) indicating the oxidation behavior of $Ce_2Zr_2O_7$ in dry air is depicted in Figure 1. It is observed that $Ce_2Zr_2O_7$ starts oxidizing just above 325 K, which implies its low thermal stability in air. It is also seen that the total mass gain occurs in two steps, that is, 1.35% in the temperature range 325−500 K and another 1.40% in the temperature range 500−873 K. The DTG curve showed a single peak in each step indicating two distinct reactions. The two-step oxidation process of $Ce_2Zr_2O_7$ observed in the present study is similar to that reported by Sasaki et al.[40] The total weight gain of 2.75% agrees well with the expected weight gain of 2.78% corresponding to the complete oxidation of Ce^{3+} to Ce^{4+}, which leads to the formation of $Ce_2Zr_2O_8$. The mass gain estimated at the intermediate step (i.e., 500 K) corresponds to gain of half of the oxygen atom, indicating the formation of an intermediate phase with composition $Ce_2Zr_2O_{7.5}$. A comparison of the observed stepwise oxidation process with that of Sasaki et al.[40,51] suggests that the composition of the intermediate phase is $Ce_2Zr_2O_{7.5}$.

The powder XRD patterns of $Ce_2Zr_2O_7$, $Ce_2Zr_2O_{7.5}$, and $Ce_2Zr_2O_8$ are shown in Figure 2. Comparison of the XRD data of these three phases indicates a close resemblance in all the reflections except systematic shifts toward higher angle due to the decrease of unit cell volume. From the position of the intense reflections, all three phases could be indexed on cubic lattices. The decrease in unit cell parameters with oxygen content can be attributed to oxidation of Ce^{3+} (radii $Ce^{3+}{}_8$ = 1.14 Å) to Ce^{4+} (radii $Ce^{4+}{}_8$ = 0.97 Å). However, the formation of distinct phases could not be confirmed from the XRD data due to the absence of any additional reflections attributable to symmetry transformation. As mentioned earlier, the X-ray diffraction pattern is excessively dominated by the scattering from the metal ions; the subtle change in structure due to oxygen stoichiometry could not be observed. Hence further structural elucidations were carried out from powder neutron diffraction data.

The Rietveld refinement of the observed powder neutron diffraction data of $Ce_2Zr_2O_7$ was carried out with the initial starting model reported for the pyrochlore ($Fd\bar{3}m$, setting II) lattice.[5] In this model, two distinct sites, namely, 16c and 16d are considered for the Zr and Ce atoms, respectively. The oxygen atoms are occupied in 48f and 8b sites. Full profile Rietveld refinements of the observed diffraction data converge successfully with the refinement of the oxygen parameter (x). It may be mentioned that the pyrochlore lattice can be explained as cubic close-packed metal ions similar to the fluorite lattice with the oxygen atoms occupying the tetrahedral interstices. The oxygen atoms of the normal pyrochlore structure fill only 7/8 (48f and 8b) of the available tetrahedral interstices leaving 1/8 (8a) as a vacant site. The disordering of the anion sites is commonly observed in several pyrochlore-type lattices having radius ratio close to the fluorite limit ($r_A/r_B < 1.4$). The crystal structure of $Ce_2Zr_2O_7$ was reported earlier by Baidya et al.[52] and

(58) Ackermann, R. J.; Chandrasekharaiah, M. S. Systematic Thermodynamic Properties of Actinide Metal-Oxygen Systems at High Temperatures, Emphasis on Lower Valence States. *Thermodynamics of Nuclear Materials*; International Atomic Energy Agency: Vienna, Austria, 1975; Vol. *II*, pp 3−26.

Table 3. Refined Positional Coordinates and Thermal Parameters of Various Atoms of $Ce_2Zr_2O_7$, $Ce_2Zr_2O_{7.5}$, and $Ce_2Zr_2O_8$

$Ce_2Zr_2O_7$

atom	site	occ.	*x*	*y*	*z*	U_{11} (Å^2)	U_{22} (Å^2)	U_{33} (Å^2)	U_{12} (Å^2)	U_{13} (Å^2)	U_{23} (Å^2)
Ce/Zr	16d	0.998/0.002	0.5	0.5	0.5	0.0071(8)	0.0071(8)	0.0071(8)	−0.0037(11)	−0.0037(11)	−0.0037(11)
Zr/Ce	16c	0.998/0.002	0	0	0	0.0133(6)	0.0133(6)	0.0133(6)	0.0051(10)	0.0051(10)	0.0051(10)
O1	48f	1	0.3432(2)	0.125	0.125	0.0371(14)	0.0078(5)	0.0078(5)	0.0	0.0	0.0011(9)
O2	8b	1	0.375	0.375	0.375	0.0137(14)	0.0137(14)	0.0137(14)	0.0	0.0	0.0

$Ce_2Zr_2O_{7.5}$

Atom	Site	occ	*x*	*y*	*z*	U_{iso} (Å^2)
Ce1	16e	1	0.1283(3)	0.1283(3)	0.1283(3)	0.0059(5)
Zr1	16e	1	0.6289(2)	0.6289(2)	0.6289(2)	0.0059(5)
O1	24f	1	0.2820(3)	0.0	0.0	0.0088(5)
O2	24g	0.96(1)	0.5071(7)	0.25	0.25	0.0088(5)
O3	4a	1	0	0	0	0.0088(5)
O4	4b	0.55(4)	0.5	0.5	0.5	0.0088(5)
O5	4c	1.00(5)	0.25	0.25	0.25	0.0088(5)
O6	4d	0.70(6)	0.75	0.75	0.75	0.0088(5)

$Ce_2Zr_2O_8$

Atom	Site	occ	*x*	*y*	*z*	*U* (Å^2)
Ce1	4a	1	0.1347(15)	0.1347(15)	0.1347(15)	0.00026
Ce2	12b	1	0.1359(13)	0.3658(16)	0.3684(15)	0.00026
Zr1	4a	1	0.6287(11)	0.6287(11)	0.6287(11)	0.00026
Zr2	12b	1	0.6232(10)	0.8729(12)	0.8656(8)	0.00026
O1	4a	1	−0.0002(16)	−0.0002(16)	−0.0002(16)	0.00083(16)
O2	4a	1	0.2553(11)	0.2553(11)	0.2553(11)	0.00083(16)
O3	4a	1	0.5051(12)	0.5051(12)	0.5051(12)	0.00083(16)
O4	4a	1	0.7369(8)	0.7369(8)	0.7369(8)	0.00083(16)
O5	12b	1	0.2511(11)	0.2607(11)	−0.0129(7)	0.00083(16)
O6	12b	1	0.2539(12)	0.2329(10)	0.5399(7)	0.00083(16)
O7	12b	1	−0.0062(11)	−0.0053(9)	0.2488(11)	0.00083(16)
O8	12b	1	−0.0044(12)	0.0000(15)	0.7645(7)	0.00083(16)

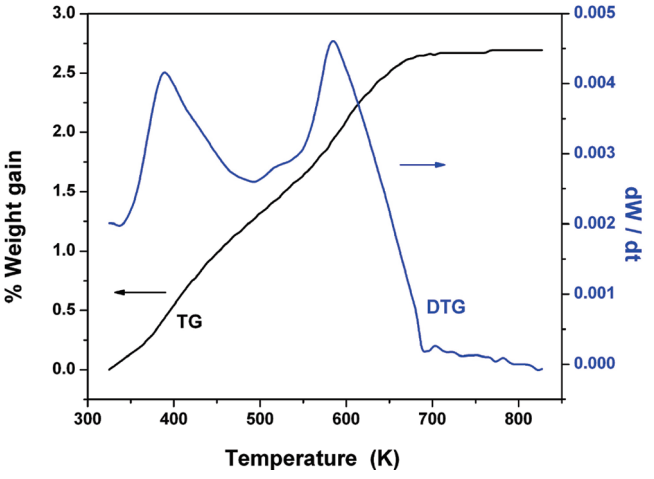

Figure 1. TG/DTG plots of oxidation of $Ce_2Zr_2O_7$ in dry air.

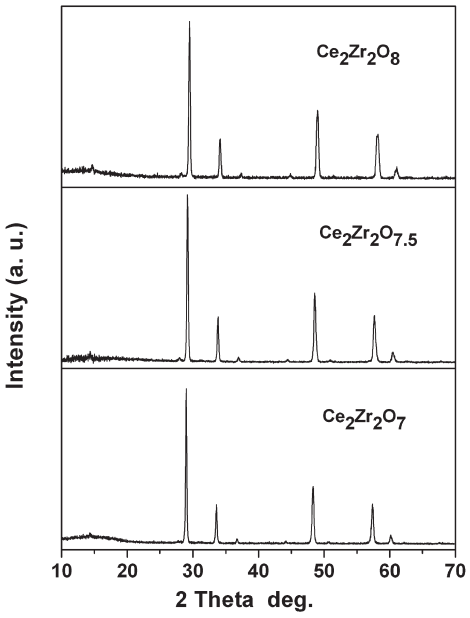

Figure 2. Powder XRD patterns of $Ce_2Zr_2O_7$, $Ce_2Zr_2O_{7.5}$, and $Ce_2Zr_2O_8$.

Sasaki et al.[51] by the Rietveld refinement of powder XRD data. The results published by Baidya et al.[52] indicate a significant disorder in the oxygen sublattice due to the anion distribution in 8b (65% occupied) and 8a (42% occupied). However, Sasaki et al.[51] reported that about 8% of 8b sites are occupied by oxygen atoms. The occupancy of the 8a site is also refined in the present study in expectation of extra oxygen atoms in the lattice. It is observed that anion occupancies at the 8a site approach negative values revealing no extra oxygen atoms in the lattice. Similar attempts with the liberation of anions from the 48f and 8b to 8a site also showed negative occupancies for the 8a site. In the expectation of possible disordering of the metal ions in the lattice, distribution of the Ce and Zr atoms at 16c and 16d sites

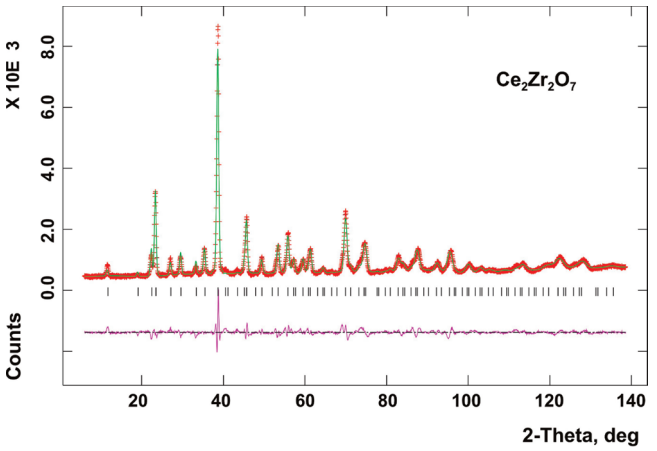

Figure 3. Rietveld refinement plots of the powder neutron diffraction data of $Ce_2Zr_2O_7$.

is attempted. The occupancies of Ce and Zr are refined with a constraint of Ce to Zr ratio as 1:1. The final occupancy of Zr in the Ce site or vice versa is not more than 0.2%, which is similar to the values reported by Sasaki et al.[51] Thus, $Ce_2Zr_2O_7$ can be considered as a fully cation-ordered lattice. Similarly, the distribution of metal ions from the present study is close to that reported by Sasaki et al.[51] but does not agree with the data reported by Baidya et al.[52] However, the present refinement of the neutron diffraction data revealed no liberated (8a) anions in $Ce_2Zr_2O_7$. The drastic difference in the distribution of anions in these studies might be an artifact of Rietveld refinement of the X-ray diffraction data. Hence, no other anion sites are considered in the final refinements. The final Rietveld refinement plot for $Ce_2Zr_2O_7$ is shown in Figure 3. The motifs of mutual adjunction of various atoms are given in Table 4. The analysis of the refined structural parameters of $Ce_2Zr_2O_7$ indicates that the cerium atoms are connected to six O1 and two O2 forming a cubic coordinated polyhedra, while six O1 atoms are coordinated octahedrally around Zr atoms. The observed Ce−O bond lengths of 2.526(1) and 2.315(1) Å and Zr−O bond lengths of 2.137(1) Å are in accordance with the eight-coordinated Ce^{3+} and six-coordinated Zr^{4+} ions. Typical interatomic distances in $Ce_2Zr_2O_7$ are given in Table 5a. The final refined coordinates of $Ce_2Zr_2O_7$ were used to generate initial models as well as to compare the structures for the successive compositions.

In an analogous manner, the powder X-ray and neutron diffraction data of the intermediate composition $Ce_2Zr_2O_{7.5}$ were analyzed. Both the powder XRD and neutron diffraction patterns of the $Ce_2Zr_2O_{7.5}$ composition do not show any significant differences from the corresponding patterns of $Ce_2Zr_2O_7$, except a decrease in the unit cell parameter and variation of intensities of several reflections. Thus, the structure was assumed to be a partially filled pyrochlore variant, without any symmetry change. Hence, Rietveld refinement of the neutron diffraction data was attempted with coordinates and symmetry of the normal pyrochlore lattice with additional oxygen atoms at the 8a site. Sasaki et al.[51] observed symmetry-forbidden reflections (200, 600, etc.) for such composition. On the basis of these reflections and electron diffraction data, a lower symmetry lattice ($F\bar{4}3m$) was assigned to $Ce_2Zr_2O_{7.5}$.[51] In order to observe the differences in the refined parameters in these two symmetries as well as to get more precise structural parameters, the present neutron diffraction data were also refined on the $F\bar{4}3m$ symmetry. The refinement based on the $Fd\bar{3}m$ symmetry shows appreciably higher residuals (R_{wp} and R_{F2}, 6.38 and 5.95) compared with that refined assuming the $F\bar{4}3m$ (R_{wp} and R_{F2}, 5.97 and 4.47). Based on the residuals of the refinement, it can be inferred that the cubic $F\bar{4}3m$ lattice is a better structural representation for $Ce_2Zr_2O_{7.5}$. The final Rietveld refinement plot of $Ce_2Zr_2O_{7.5}$ is shown in Figure 4. The refined structural parameters are summarized in Tables 2 and 3.

The analysis of the structural parameters revealed that the lowering of symmetry from $Fd\bar{3}m$ to $F\bar{4}3m$ resulted from the splitting of the 48f anion site into two sets, namely, O1 (24f) and O2 (24g). However, the ordering of the metal ions remains similar to that in the parent lattice. Also the splitting of the anion sites corresponding to 8b and 8a to O3 (4a), O5 (4c) and O4 (4b), O6 (4d) occurs in the $F\bar{4}3m$ symmetry. Thus, six distinct anion sites, namely, O1−O6 are considered in the structure of the $Ce_2Zr_2O_{7.5}$ composition. The motifs of mutual adjunction of various atoms in the structure of $Ce_2Zr_2O_{7.5}$ are given in Table 4. The fractional occupancies of various anion sites are given in Table 3. The composition $Ce_2Zr_2O_{7.52}$ obtained from the refined occupation numbers is in close agreement with the composition $Ce_2Zr_2O_{7.5}$ obtained from thermogravimetry. The occupancies of various anion sites indicate that the anion sites corresponding to the normal pyrochlore lattice are almost filled while sites 4a and 4d equivalent to the empty 8a sites are partially occupied. Thus, the crystal structure of $Ce_2Zr_2O_{7.5}$ represents a filled variant of the $Fd3m$ lattice of $Ce_2Zr_2O_7$. The overall arrangement of the various atoms in these two does not show appreciable difference except a shift in positions due to extra interstitial anions.

The analysis of the refined structural parameters of $Ce_2Zr_2O_{7.5}$ indicates that the cerium atoms are connected to three O1 and three O2 atoms forming an octahedral coordination. The typical Ce−O1 and Ce−O2 distances are 2.525 and 2.326 Å, respectively. Two opposite faces of the CeO_6 octahedra formed by O1 and O2 are capped with O3 and O5 atoms forming an eight-coordinated CeO_8 polyhedra. The average Ce−O distance in $Ce_2Zr_2O_{7.5}$ is 2.394 Å, which is in accordance with the Ce^{4+}−O (2.343 Å)[59,60] and Ce^{3+}−O (2.475 Å).[49] Similar eight-coordinated polyhedra around the Zr atoms are formed with three O1, three O2, and one each of O4 and O6 atoms. As mentioned earlier, the O4 and O6 atoms, which are equivalent to the vacant (8a) sites of the pyrochlore lattice are partially occupied. The average

(59) Mulford, R. N. R.; Ellinger, F. H. *J. Phys. Chem.* **1958**, *62*, 1466.
(60) Wyckoff, R. W. G. *Crystal Structures*, 2nd ed.; Interscience Publishers: New York, 1963; Vol. *1*, p 239.

Table 4. Motif of Mutual Adjunction of Various Atoms in $Ce_2Zr_2O_7$, $Ce_2Zr_2O_{7.5}$, and $Ce_2Zr_2O_8$

$Ce_2Zr_2O_7$

	O1	O2	void	CN
Ce1	6/2	2/4	0/0	8
Zr1	6/2	0/0	2/4	8
CN	4	4	4	

$Ce_2Zr_2O_{7.5}$

	O1	O2	O3	O4	O5	O6	CN
Ce1	3/2	3/2	1/4	0/0	1/4	0/0	8
Zr1	3/2	3/2	0/0	1/4	0/0	1/4	8
CN	4	4	4	4	4	4	

$Ce_2Zr_2O_8$

	O1	O2	O3	O4	O5	O6	O7	O8	CN
Ce1	1/1	1/1	0/0	0/0	3/1	0/0	3/1	0/0	8
Ce2	1/3	1/3	0/0	0/0	1/1	2/2	1/1	2/2	8
Zr1	0/0	0/0	1/1	1/1	3/1	0/0	3/1	0/0	8
Zr2	0/0	0/0	1/3	1/3	1/1	2/2	1/1	2/2	8
CN	4	4	4	4	4	4	4	4	

Table 5. Typical Bond Distances (Å) of Various Atoms in $Ce_2Zr_2O_7$, $Ce_2Zr_2O_{7.5}$, and $Ce_2Zr_2O_8$

$Ce_2Zr_2O_7$		$Ce_2Zr_2O_{7.5}$		$Ce_2Zr_2O_8$			
Ce−O1 × 6	2.526(1)	Ce−O1 × 3	2.525(3)	Ce1−O1 × 1	2.46(4)	Zr1−O3 × 1	2.257(22)
Ce−O2 × 2	2.315(1)	Ce−O2 × 3	2.326(5)	Ce1−O2 × 1	2.202(33)	Zr1−O4 × 1	1.977(22)
		Ce−O3 × 1	2.360(6)	Ce1−O5 × 1	2.306(12)	Zr1−O5 × 3	2.244(13)
		Ce−O5 × 1	2.239(6)	Ce1−O5 × 2	2.386(12)	Zr1−O7 × 3	2.320(10)
				Ce1−O7 × 3	2.415(12)		
Zr−O1 × 6	2.137(1)	Zr−O1 × 3	2.155(3)				
		Zr−O2 × 3	2.232(5)	Ce2−O1 × 1	2.444(12)	Zr2−O3 × 1	2.373(10)
		Zr−O4 × 1	2.371(5)	Ce2−O2 × 1	2.089(12)	Zr2−O4 × 1	2.310(10)
Zr-(v) × 2[a]	2.315(1)	Zr−O6 × 1	2.227(5)	Ce2−O5 × 1	2.283(18)	Zr2−O5 × 1	2.071(16)
				Ce2−O6 × 1	2.605(18)	Zr2−O6 × 1	1.942(16)
				Ce2−O6 × 1	2.423(22)	Zr2−O6 × 1	2.202(14)
				Ce2−O7 × 1	2.290(17)	Zr2−O7 × 1	2.234(12)
				Ce2−O8 × 1	2.214(20)	Zr2−O8 × 1	2.429(16)
				Ce2−O8 × 1	2.292(25)	Zr2−O8 × 1	2.434(18)

[a] v = vacancy.

Zr−O bond length observed in such eight-coordinated polyhedra is 2.220 Å, which is in accordance with eight-coordinated polyhedra of the tetragonal ZrO_2,[61] as well as κ-$CeZrO_4$.[53]

Similar to the powder XRD pattern of $Ce_2Zr_2O_{7.5}$, the powder XRD pattern of $Ce_2Zr_2O_8$ also does not reveal any drastic differences from that of $Ce_2Zr_2O_7$. A comparison of the powder neutron diffraction data of $Ce_2Zr_2O_8$ with those of $Ce_2Zr_2O_7$ and $Ce_2Zr_2O_{7.5}$ shows additional weak reflections not accountable with the face-centered lattice of the latter two. All the observed reflections including the weak reflections could be indexed on a primitive cubic lattice. It was reported that about 20% of ZrO_2 can be retained in the fluorite lattice of the CeO_2 without any distortion.[62] Several reports also demonstrated the formation of a fluorite-type solid solution lattice for $Ce_2Zr_2O_8$ in both low-temperature[52] and high-temperature synthesis conditions.[63] $Ce_2Zr_2O_8$ composition prepared by conventional solid-state reaction of

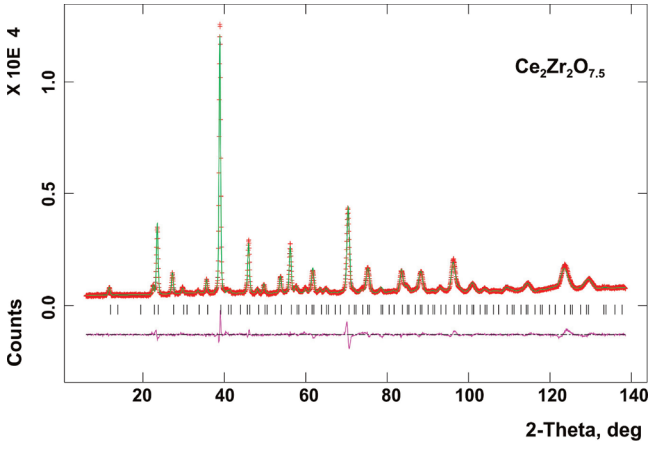

Figure 4. Rietveld refinement plots of the powder neutron diffraction data of $Ce_2Zr_2O_{7.5}$.

(61) Igawa, N.; Ishii, Y.; Nagasaki, T.; Morii, Y.; Funahashi, S.; Ohno, H. *J. Am. Ceram. Soc.* **1993**, *76*, 2673.
(62) Yashima, M.; Arashi, H.; Kakihana, M.; Yoshimura, M. *J. Am. Ceram. Soc.* **1994**, *77*, 1067.
(63) Tani, E.; Yoshimura, M.; Somiya, S. *J. Am. Ceram. Soc.* **1983**, *66*, 506.

CeO_2 and ZrO_2 mostly resulted in a mixture of cubic and tetragonal phases[64] or tetragonally distorted t or t′ $CeZrO_4$ phases.[54−56,62] The weak reflections observed in the powder XRD pattern of $Ce_2Zr_2O_8$ attributable to pyrochlore-type ordering discards the fluorite-type solid solution lattice[52] as well as the tetragonally distorted t or t′ $CeZrO_4$ phases.[54−56,62] The retention of the pyrochlore-type cation ordering can be attributed to a facile intercalation of oxygen into the lattice, without disturbing the cationic sublattice. Such an oxygen intercalated pyrochlore lattice of $Ce_2Zr_2O_8$ was reported as κ-$CeZrO_4$[53] with cubic lattice ($P2_13$) from powder XRD studies. However, the powder neutron diffraction data of a closely related composition $Ce_2Zr_2O_{7.94}$ was explained by a feebly distorted rhombohedral ($R\bar{3}m$) lattice.[50] It can be mentioned here that the observed reflections in the neutron diffraction pattern can be accounted in both rhombohedral and cubic lattices. The model parameters for the symmetry-related crystal structures can be derived by group−subgroup relations and thus initial coordinates for possible models were derived from the parent pyrochlore lattice ($Fd3m$). The sequences of adopted symmetry transformation from pyrochlore to other considered lattices are given below. Such symmetry transitions were also followed by Thomson et al.[50] for $R\bar{3}m$ and Kishimoto et al.[53] for $P2_13$ lattices. Thus, the Rietveld refinement of the powder neutron diffraction data of $Ce_2Zr_2O_8$ was carried out on both the rhombohedral and the cubic models.

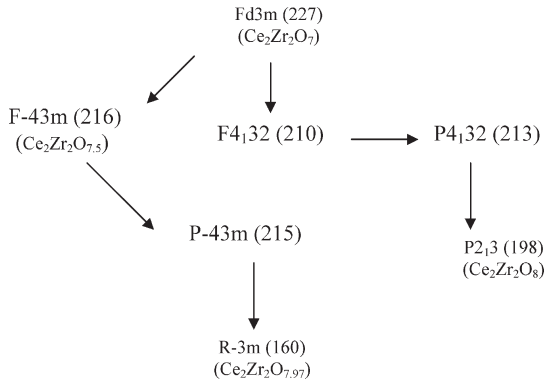

The rhombohedral lattice ($R\bar{3}m$) proposed by Thomson et al. for $Ce_2Zr_2O_{7.97}$[50] composition has 11 anion sites versus eight anion sites for cubic κ-$CeZrO_4$.[53] Besides, Thomson et al. considered a partially occupied anion site with coordination number three in the structure model.[50] It may be noted here that significantly reduced interanion distances arising due to this anion site lead to sterically hindered oxidation. However, the present oxidation studies of $Ce_2Zr_2O_7$ indicate no such hindered oxidation process, which is similar to the observations of Sasaki et al.[40,51] Thus such an anion site is less likely to be present in the crystal structure. This is further confirmed from the Rietveld refinements of neutron diffraction studies based on both rhombohedral and cubic model structures.

(64) Varez, A.; Garcia-Gonzalez, E.; Sanz, J. *J. Mater. Chem.* **2006**, *16*, 4249.

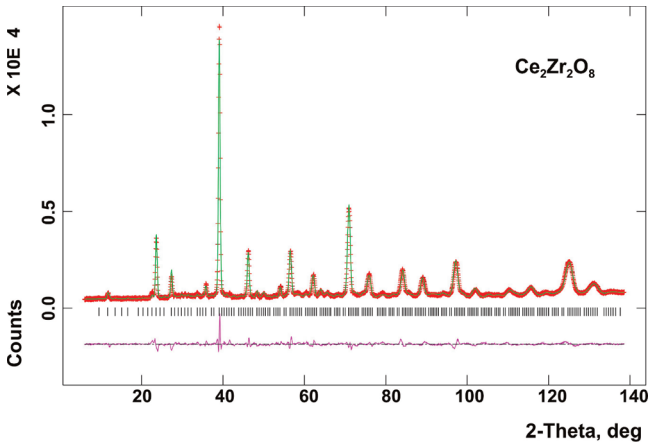

Figure 5. Rietveld refinement plots of the powder neutron diffraction data of $Ce_2Zr_2O_8$.

The final residuals (R_{wp} and R_p) of the Rietveld refinements show higher values for rhombohedral lattice (7.08% and 5.27%) compared with those for cubic lattice (6.64% and 5.00%). The calculated intensities of several reflections, in particular, weak reflections, show appreciable differences from the observed ones. The Rietveld analyses of the powder ND data refined on the cubic ($P2_13$) lattice show appreciably good profile match, as well as better residuals of refinements. The final Rietveld refinement plot is shown in Figure 5. Hence, we conclude that the fully oxidized cubic κ-$Ce_2Zr_2O_8$ lattice is formed in the oxidation process. The residuals of refinements and refined position coordinates are given in Tables 2 and 3, respectively.

The analysis of the refined structural parameters of $Ce_2Zr_2O_8$ shows that Ce and Zr sites of the parent pyrochlore lattice split into two different sites (4a and 12b). Similarly, four oxygen atoms (O1−O4) are occupied in 4a sites, while the other four (O5−O8) are occupied in 12b sites. Each of the anions is tetrahedrally coordinated like the normal fluorite or pyrochlore lattice. Both Ce and Zr atoms form eight-coordinated polyhedra with oxygen atoms similar to the fluorite structure. The typical motifs of mutual adjunction of various atoms are given in Table 4. The observed Ce1−O and Ce2−O bond lengths are in the range of 2.20−2.46 and 2.29−2.61 Å, respectively. The variation of the Ce−O bond lengths around Ce1 and Ce2 indicates the Ce2 atoms form a more distorted cube compared with the Ce1. Similar analysis of the interatomic bond distances (Table 5) around Zr1 and Zr2 indicates that $Zr(2)O_8$ units are more distorted than the $Zr(1)O_8$ polyhedral units. Both CeO_8 and ZrO_8 units are connected by sharing all 12 edges forming the three-dimensional lattice (Figure 6). For comparison, the crystal structure of $Ce_2Zr_2O_7$ is also included in Figure 6.

A comparison of the structures of $Ce_2Zr_2O_7$, $Ce_2Zr_2O_{7.5}$, and $Ce_2Zr_2O_8$ indicates that the typical arrangements of various atoms are similar except for the partially occupied anion sites in $Ce_2Zr_2O_{7.5}$, vacant anion sites in $Ce_2Zr_2O_7$, and fully occupied anion sites in $Ce_2Zr_2O_8$. Considering the anions and vacancies, all the three structures have cubical coordinated polyhedra around Ce or

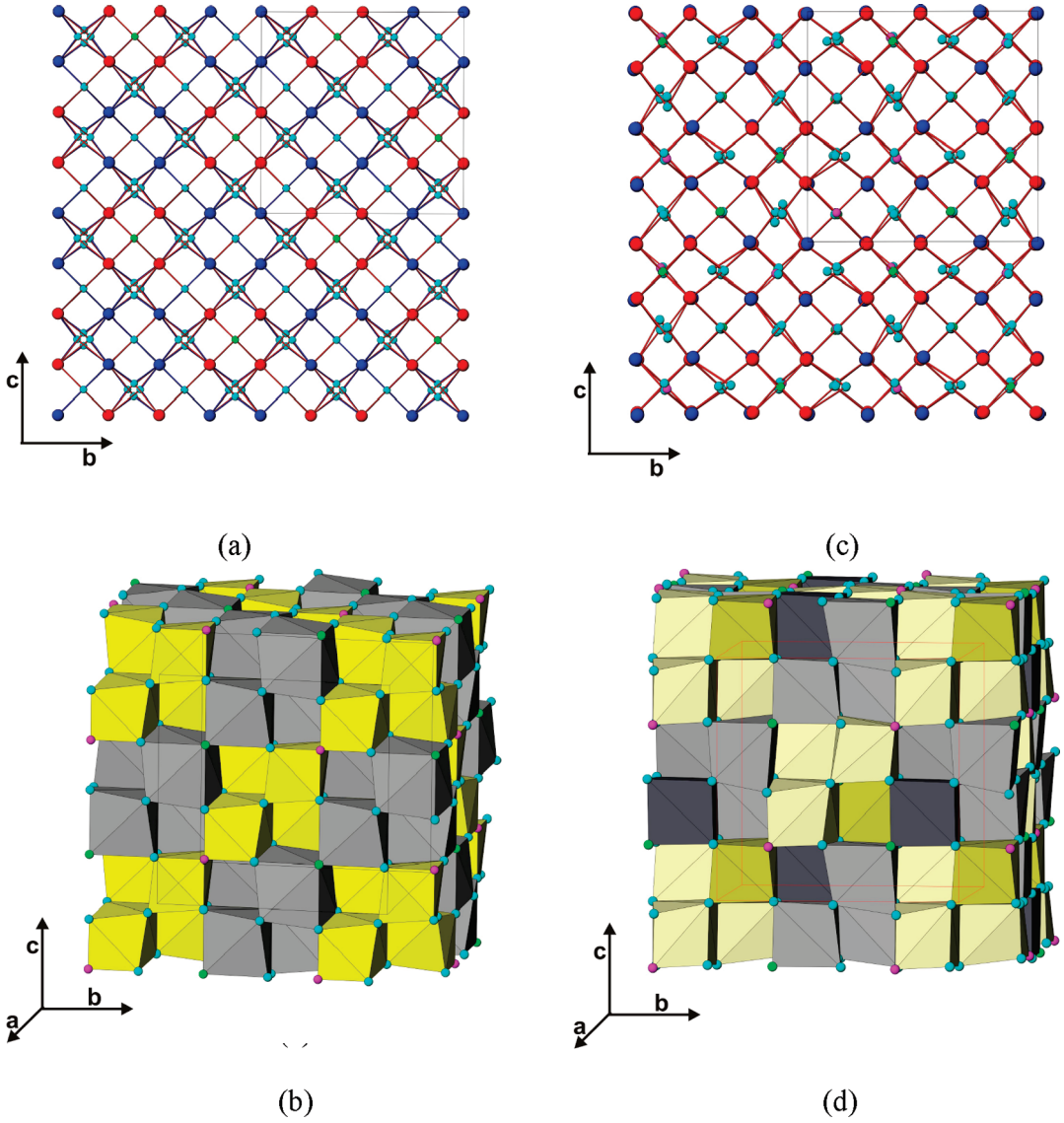

Figure 6. Crystal structures of $Ce_2Zr_2O_7$ (a, b) and $Ce_2Zr_2O_8$ (c, d). Red and dark blue spheres represent Ce and Zr atoms, small light blue spheres represent oxygen atoms in parts a and c, yellow and gray cubes represent CeO_8 and $ZrO_6[\square]_2$, units in parts b and d. ($\square$ = vacancy in part b and oxygen in part d).

Zr atoms, and they are arranged in a similar manner to the fluorite lattice. The CeO_8 and ZrO_8 or $ZrO_6[V]_2$ cubes share their edges to form a fluorite-type lattice. The typical coordination polyhedra around the metal atoms and their representative connections are shown in Figure 7. The variations of local structures with the change in oxygen stoichiometry are also illustrated in Figure 7.

It is well-known that the pyrochlore structure is closely related to the fluorite structure. The fluorite structure can be transformed to the pyrochlore structure and vice versa with the change in cation ordering and filling of oxygen vacancy [V] (marked as O3 in Figure 7). In order to compare the structural transformation with the oxygen stoichiometry in $Ce_2Zr_2O_7$ to $Ce_2Zr_2O_8$, all the three structures are compared on the basis of coordinates of a typical cation-ordered ideal fluorite lattice. The relations of positional coordinates of these studied compositions are depicted in Figure 7. The sequential transformation of crystal structure is mainly reflected in the oxygen atoms without any significant disturbance in the metal ion positions. This cation ordering is reflected in the shift (x) of the oxygen sites from normal fluorite positions of O1 atoms. In ideal fluorite-type arrangement, the value of x is 0.375, which shifts to 0.3125 for an ideal octahedral coordination around the smaller cation (16c cation) in the pyrochlore structure. The present observed value of x = 0.3432 in $Ce_2Zr_2O_7$ indicates a nearly ideal octahedron around the Zr atom. The shift of this oxygen mainly depends on the ionic radii of the cations. The analysis of the observed positional coordinates of various atoms with their ideal values shows that both cations and anions shift from their ideal values due to the incorporation of extra oxygen in the lattice. The typical shifts of various atoms in $Ce_2Zr_2O_7$, $Ce_2Zr_2O_{7.5}$, and $Ce_2Zr_2O_8$ with respect to the corresponding arrangements in undistorted fluorite type lattices are shown in Figure 8. The analysis of the shifts of various atoms in $Ce_2Zr_2O_{7.5}$ with respect to the fluorite lattice shows that both the metal ions shift along the ⟨111⟩ directions while the anions O1 and O2 shift along ⟨100⟩

directions. The extent of shift of the O1 is significantly larger (~0.3 Å) than that of the O2 (0.07 Å). Such arrangements of the atoms destroy the *d*-glide symmetry of the pyrochlore lattice, retaining all other symmetry elements, and thus show only a small difference in the structures. Similar comparison of the structural parameters of the $Ce_2Zr_2O_8$ with the ideal position coordinates revealed shifts in all the atoms. In the oxidation process of Ce^{3+} to Ce^{4+}, the cations also shifted in two different sites depending on the anion environment. Similarly, the position coordinates of the Zr1 and Zr2 atoms are moved from the ideal position but to a lesser extent than the Ce atoms. Among the anions, the anions surrounding the Zr atoms are influenced significantly by such an oxidation process, which can also be expected from the difference in their coordination polyhedra. Thus, it can be inferred that the $Ce_2Zr_2O_8$ and $Ce_2Zr_2O_{7.5}$ have oxygen intercalated lattices.

The cation ordering obviously resulted from the size and charge difference in Ce and Zr of $Ce_2Zr_2O_7$. The same arrangement is retained during the oxidation process also. The oxidation of Ce^{3+} to Ce^{4+} intercalates extra oxygen atoms to fill the vacant sites of the pyrochlore lattice. Usually, such an oxidation process has lower activation energy and hence favors the formation of the oxygen-rich pyrochlore lattice of $Ce_2Zr_2O_8$. Since this process occurs at significantly lower temperature, the cation migration or interdiffusion to form the cation disordered t- or c-$CeZrO_4$ lattice is not favored. Thus the solid solution of CeO_2 and ZrO_2 either in the cubic (c) or in the tetragonal (t, t′) lattice occurs only in the process of high-temperature reactions. According to the CeO_2–ZrO_2 phase diagram,[61,64] the fluorite-type solid solution can form at $0.5CeO_2$–$0.5ZrO_2$ only above 2000 K, where cation interdiffusion can occur. However, the observation of fluorite-type solid solution in the nanoregime has been confirmed in several studies.[30–37,43,44,52]

The reduction studies of the $Ce_2Zr_2O_8$ phase carried out by thermogravimetry in 8% H_2 in an argon atmosphere (Figure 9) indicate the onset of release of oxygen at 973 K, and the rate of release is appreciably faster around 1273 K. The total mass loss observed in the temperature

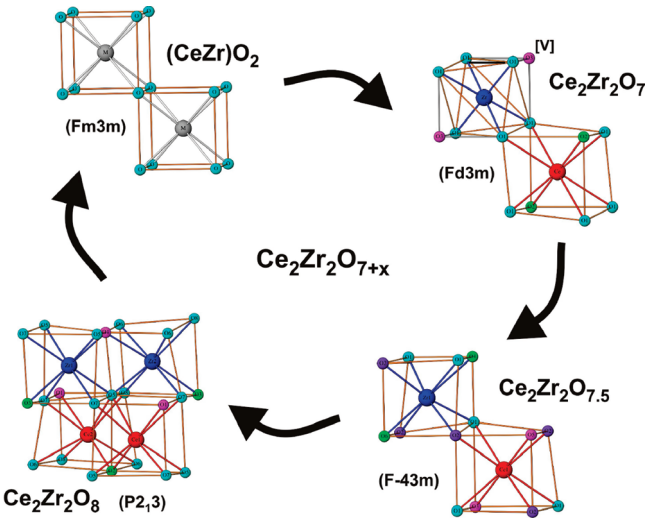

Figure 7. Structural transformations in $Ce_2Zr_2O_7$, $Ce_2Zr_2O_{7.5}$, and $Ce_2Zr_2O_8$.

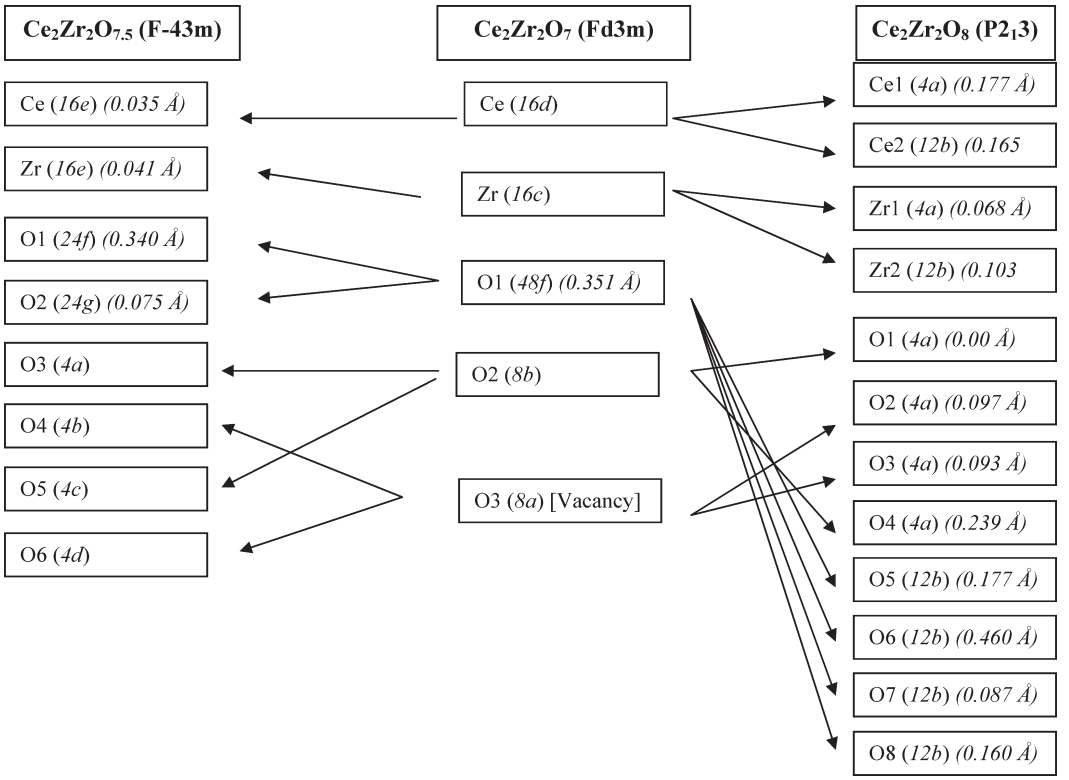

Figure 8. Atomistic relation and Wyckoff sites in the structures of $Ce_2Zr_2O_7$, $Ce_2Zr_2O_{7.5}$, and $Ce_2Zr_2O_8$. Numerals in italics indicate the shift of atoms from the ideal fluorite arrangements.

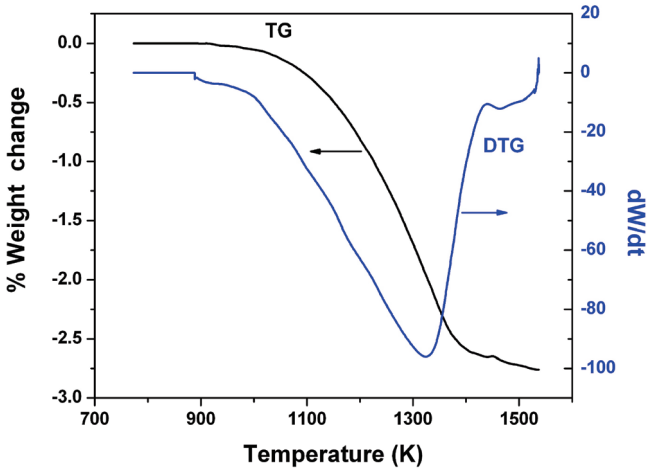

Figure 9. TG/DTG plots of $Ce_2Zr_2O_8$ under flowing atmosphere of 8% v/v hydrogen−argon gas mixture.

range of 973 to 1423 K is 2.7%, which corresponds to the formation of $Ce_2Zr_2O_7$ (expected mass loss 2.708%). The residue obtained after complete reduction could also be identified as $Ce_2Zr_2O_7$ from its XRD data. The DTG of the reduction process up to 1423 K indicates that the total mass loss from Ce^{4+} to Ce^{3+} occurs in a single step without formation of intermediate $Ce_2Zr_2O_{7.5}$ composition. This can be attributed to the higher reduction potential of hydrogen, which could not stabilize the intermediate phase. The reduction to $Ce_2Zr_2O_{6.2}$ from fluorite type CeO_2-ZrO_2 solid solution (mass loss ≈ 5%) reported by Baidya et al.[52] might be due to other effects, like higher reactivity and disorder, besides the crystal structure. Also prolonged reduction of fluorite-type CeO_2-ZrO_2 solid solutions under pure hydrogen causes such reduction at relatively lower temperature.[52] Besides, the reduction of $Ce_2Zr_2O_8$ at relatively lower temperature than that expected for pure CeO_2 can be attributed to the distortion in the lattice and disorder in the anion sites, as observed from the crystal structure data. The significant variations of bond lengths in the coordination polyhedra around Ce and Zr atoms favorably release the oxygen from the lattice.

It has been mentioned in the Introduction section that the redox behavior of CeO_2-ZrO_2 shows a distinct onset of reduction temperature with severe or mild oxidizing pretreatment after a severe reduction. The onset temperature of reduction increases from about 840 K for a fresh sample to higher temperature (~900−950 K) when it is subjected to severe oxidation conditions after a pre reduction.[21,22,32−34,38] On the other hand, the onset temperature decreases below 840 K after a mild oxidation of a pre-reduced sample.[21,22,32−34,38] Our studies revealed that reduction behavior is initiated at 973 K (Figure 9), which agrees well with severe redox-treated cases of these reports. A comparatively higher observed temperature (973 K) for reduction in the present investigation might be attributed to the low surface area due to highly crystalline nature of the sample.

The microstructural characterizations of the samples conditioned under various redox treatments indicate that the cation sublattice is retained in the pyrochlore-based samples[42−51] while the cation ordering originates at a relatively lower temperature for fluorite-based samples.[21,22,32−38,43,44,51] Thus the formation of pyrochlore-like ordered lattice is evident in the redox process of CeO_2-ZrO_2 samples. The destruction of the pyrochlore-type cation ordering has been reported under severe (high temperature, > 1323 K) oxidation conditions leading to new tetragonal (t*) phases.[54−56,62] Vlaic et al.[20] and Fornsiero et al.[33,38] have investigated the local structure fluorite-type CeO_2-ZrO_2 solid solutions and observed a significant disorder in the anion (oxygen) sublattice on CeO_2-ZrO_2 system. These reports relate the reduction behavior of the CeO_2-ZrO_2 system to the anion disorder. Montini et al.[22] have explained the nucleation of pyrochlore-type ordering at the surface and growth to the bulk at higher temperature and higher hydrogen concentration. They attributed the formation of pyrochlore lattice to an effect of the reduction. Alessandri et al.[39] have also suggested that the formation of pyrochlore-type cation ordering initiates after a reduction treatment. Detailed microscopic investigations by Yeste et al.[30] and Perez-Omil et al.[44] show a clear evidence of the cation-ordered lattice for low-temperature reduced CeO_2-ZrO_2 solid solution samples. The redox behavior remains similar even after repeated cycles. The difference in reduction behavior under mild and severe oxidizing treatment after a severe reduction step suggests a close link to the redox behavior of the pyrochlore phase.

During the oxidation process of the pyrochlore phase of $Ce_2Zr_2O_7$, two distinct structure types ($Ce_2Zr_2O_{7.5}$ and $Ce_2Zr_2O_8$) were observed without the destruction of the cation ordering. The lower reduction temperature of mild oxidation samples might originate from the highly anion-disordered defect structure of $Ce_2Zr_2O_{7.5}$, while the increase in reduction temperature after severe oxidizing pretreatment arises from the $Ce_2Zr_2O_8$. In both the cases, a facile deintercalation of oxygen is expected due to the distortion in the lattice and disorder in the anion sites. The partial oxygenation of $Ce_2Zr_2O_7$ leads to the formation of a $Ce_2Zr_2O_{7.5}$-type structure, where the vacant oxygen sites make a possible channel for oxygen diffusion in the lattice, which favors the reduction. Arai et al.[46−48] have reported oxygen-deficient alternated planes parallel to (100) plane. The two partially occupied oxygen sites (O4 and O6) of the refined $Ce_2Zr_2O_{7.5}$ structure in the present investigation indicate the formation of a corrugated oxygen row along the ⟨010⟩ direction, hence favoring the diffusion of oxygen in the lattice. Fornasiero et al.[34] have earlier established that in the mild oxygenated sample the reduction behavior is related to the oxygen diffusion in the lattice, which is in agreement with the results observed in the present study as well as that of Arai et al.[46−48] However, the diffusion of oxygen in the $Ce_2Zr_2O_8$-type arrangement is expected to be lower than that in $Ce_2Zr_2O_{7.5}$, due to completely filled anion sites. The highly disordered coordination polyhedra with appreciably larger M−O bonds favor reduction compared with the parent fluorite or pyrochlore phase.

Similar dispersion of bond lengths have been earlier concluded from an EXAFS study on a fluorite-type solution of CeO_2-ZrO_2.[20,33,38] In this case, higher reduction temperature can be expected due to the breaking of metal−oxygen bonds for reduction. This is in accordance with the reduction mechanism of $Ce_{0.5}Zr_{0.5}O_2$ after a severe reduction followed by severe oxidation treatment.[34] In conclusion from the present crystal chemical studies on $CeO_2-Ce_2O_3-ZrO_2$ system, it is observed that $Ce_2Zr_2O_7$ transforms to easily reducible distorted structures on oxidation. These deep crystallographic insights will pave the way for the development of a pyrochlore-based efficient redox catalyst.

4. Conclusions

The crystal structures of $Ce_2Zr_2O_7$, $Ce_2Zr_2O_{7.5}$, and $Ce_2Zr_2O_8$ have been accurately determined from the neutron diffraction of polycrystalline samples. The unit cell parameters systematically decreased from $Ce_2Zr_2O_7$ to $Ce_2Zr_2O_8$, retaining the cubic lattice. All three compositions retained the original pyrochlore-type cation ordering without any intermixing between Ce and Zr atoms. All three structures can be explained as cubically coordinated AO_8 polyhedra around the metal atoms, which share all the edges similar to those in the fluorite lattice. The precise location of cation and anions and their comparison to the parent fluorite lattice unraveled the sequential structural transformation with oxygen stoichiometry. The transformation from $Ce_2Zr_2O_7$ to $Ce_2Zr_2O_8$ systematically lowers the symmetry from $Fd3m$ to $P2_13$. A complete oxidation of Ce^{3+} to Ce^{4+} is observed in contrast to the kinetically and sterically hindered oxidation proposed by other researchers. The structural results obtained from this study provide sufficient clues to the easy oxygen uptake and release behavior of the cerium zirconates.

Acknowledgment. The authors thank Dr. D. Das, Head, Chemistry Division, for his support of this work. Also the authors thank Dr. S. K. Aggarwal, Head, Fuel Chemistry Division, for fruitful discussions and valuable suggestions on the manuscript.

Supporting Information Available: Crystallographic information files (CIF format) for $Ce_2Zr_2O_7$ (CSD-420822), $Ce_2Zr_2O_{7.5}$ (CSD-420823) and $Ce_2Zr_2O_8$ (CSD-420824) for the neutron diffraction data at ambient temperature. This information is available free of charge via the Internet at http://pubs.acs.org.